Korean J. Chem. Eng., 33(3), 922-933 (2016)
DOI: 10.1007/s11814-015-0188-6

pISSN: 0256-1115
eISSN: 1975-7220

Process modeling and optimization of Rhodamine B dye ozonation in a novel microreactor equipped with high frequency ultrasound wave

Mahboubeh Faryadi, Masoud Rahimi†, and Mona Akbari

CFD Research Center, Chemical Engineering Department, Razi University, Kermanshah, Iran
(*Received 19 May 2015 • accepted 28 August 2015*)

Abstract−This paper reports the effect of 1.7 MHz ultrasound wave on decolorization efficiency of Rhodamine B (RB) solution by ozone in a T-type microreactor. Response surface methodology using central composite design (CCD) was used for analysis and optimization of the reaction conditions. The effective parameters such as solution pH, dye initial concentration, liquid volumetric flow rate, ozone dosage and the length of microreactor on decolorization process were investigated. Rhodamine B removal from solution was determined in presence of and without sonication. The results indicate that for both modes, the decolorization efficiency of RB increased with increase of the ozone dosage as well as the length of employed microreactor. However, with increase of RB initial concentration and liquid flow rate, the decolorization efficiency was decreased. The comparison between the reactors with and without sonication shows that the application of ultrasound wave is effective more than 15% on removal efficiency of RB at various conditions. At optimum conditions, the experimental RB removal yield of 97.3% and 95.8 was obtained for with and without irradiation layouts, respectively. The statistical analyses and the agreement of the experimental results with model predictions showed the reliability of the regression model.

Keywords: Decolorization, Microreactor, Optimization, Ozonation, Rhodamine B

INTRODUCTION

One of the major environmental problems is textile industry wastewater that contains high concentration of complex organic dyes. Azo dyes are chemical components containing azo groups (-N=N-) bond to benzene or naphta rings in their structure [1]. There are several applied treatment methods for textile effluents, involving physical and chemical methods. Some of these methods have been reported to treat the textile effluents containing azo dyes: adsorption, flocculation, coagulation, photocatalytic and Fenton oxidation methods [2-6]. The main problems of these approaches are high operational costs, long reaction time and secondary pollution. Therefore, finding a convenient method to wastewater treatment technology and solving these problems is required [7,8]. One quick and effective process to treat wastewater is ozonation [9-12]. Some researchers have begun to focus on using ozonation to remove several kinds of azo dyes [9,10,13-15]. The ozonation process is related to both kinetic reactions and the transfer between phases. Ozone mass transfer rate from the gas phase to the gas-liquid interface due to the low solubility in water may be the rate-limiting step in the ozonation process of wastewater. Mass transfer rate in this process strongly depends on the mixing performance of gas-liquid contactor (LPC). Therefore, the design and application of a gas-liquid contactor system for better mass transfer performance is needed [9,16,17]. In recent years, some researchers have tried to employ microtechnology (using micro-scale equipment in a process) with great potential performance in many industrial processes. Microstructured reactors are generally three-dimensional structures with dimensions in micrometer scale, with extremely large surface to volume ratio. The short transport path in microchannels increases the heat and mass transfer rate significantly compared with conventional LPC and reactors [18,19]. The miniaturization of chemical reactors also has many other benefits including minimal environmental hazards and increased safety due to the smaller volume besides reduction of process costs [20-22]. According to the reported results, the mass transfer rate between gas-liquid is greatly increased in comparison to conventional gas-liquid contactors [9]. Most of the reported studies on the removal dyes were carried out in microchannels for liquid-liquid systems [23-25]. However, there are limited numbers of studies on using microchannels on dye removal in the gas-liquid process. Gao et al. [26] expressed removal of Azo dye Acid Red 14 by ozone process in a microporous tube in tube micoreactor. Their results demonstrated that with an increase in ozone gas flow rate, with reduction of initial AR 14 concentration and liquid flow rate, the removal efficiency was enhanced significantly [9]. In our previous work [27], an investigation was carried out on different types of microchannels irradiated with a piezoelectric transducer (PZT) with a frequency in range of MHz waves, which in this range are capable of producing cavitation, which can improve micromixing in this type of reactor. The implosive collapse of microbubbles results in a variety of mechanical effects such as micro-streaming and micro-jet that have ability to increase the mass transfer rate and cause a turbulence-jet in a fluid. Some researchers tried to use ultrasound techniques for improving the micromixing in various reactors geometric such as semi-batch reactor [28,29] and continuous reactor [30,31]. In most of these inves-

†To whom correspondence should be addressed.
E-mail: m.rahimi@razi.ac.ir, masoudrahimi@yahoo.com

tigations low frequency (in range of kHz) ultrasound waves in direct contact with fluids were used. Based on this previous research, it can said that development of the combined microreactor with high frequency ultrasound waves of 1.7 MHz can be effective for enhancing micromixing and mass transfer rate between the gas-liquid interface. Also, according to the mechanism of degassing, at high frequency of 1.7 MHz with low power intensity, the degassing in the system is very weak [32] due to creation of very small bubbles.

One of the important dyes widely used in the textile industry is Rhodamine B (RB). Some studies have been carried out using few methods for removal of Rhodamine B (RB) from wastewater. Removal of RB by using swirling jet-induced cavitations combined with H_2O_2 was reported by Wang et al. [33]. Chang et al. [34] investigated removal by fly ash adsorption with Fenton pre-oxidation. Kumal et al. [35] presented photo Fenton reagent. Garg et al. [36] expressed removal of RB from aqueous solution by adsorption of timber industry waste. Photocatalytic degradation of Rhodamine B under UV-Visible light irradiation using different nanostructured catalysts was done by Del C et al. [37]. Mcheik et al. [38] studied the decolorization of RB with persolfate by spectrophotometric methods. Also, Cuiping et al. [10] investigated its removal by ozone-based advanced oxidation process in the batch reactor. However, using these methods can cause problems such as high operational costs, secondary pollution and long reaction time. In this research, we have investigated the RB removal and reduction of reaction time by a novel combined microreactor with ultrasound waves of high frequency in range of MHz, which can increase micromixing and improve mass transfer rate between ozone and liquid phase.

On the other hand, response surface methodology (RSM) is an advanced tool in process design and optimization of operating condition [39]. In recent years, RSM has been applied as well to optimize and evaluate the interactive effects of independent factors in chemical processes [40-44]. Thereby, in this research RSM based on central composite design (CCD) was used to analyze the influence of process variables on removal efficiency of RB and to optimize conditions in the studied microreactor.

Our main aim was to investigate the removal of azo dye RB from solution using microreactor by ozonation process. The microreactor was placed in an ultrasonic container equipped with high frequency (1.7 MHz) piezoelectric transducer to evaluate the effect of ultrasonic waves in enhancing ozone mass transfer rate in gas-liquid interface. In this work, the influences of different parameters such as length of microreactor, initial concentration of RB, initial pH solution, liquid volumetric flow rate and ozone-containing gas volumetric flow rate on decolonization efficiency were investigated. The effects of these operating variables on decolonization efficiency in presence and without ultrasound waves were analyzed. Furthermore, we tried to find optimum conditions and achieve the maximum efficiency of RB decolorization by using RSM technique.

MATERIAL AND METHODS

1. Materials

An azo dye Rhodamine B (RB) with chemical formulation of $C_{28}H_{31}ClN_2O_3$ and molecular weight of 479.02 was supplied from Fluka and used without further purification. Deionized water was used for preparing solutions containing 50, 65 and 80 ppm of RB. The solution pH was adjusted using 0.1 M NaOH or H_2SO_4. Sulfuric acid with a purity of 98% was also provided from Fluka. All other chemical materials used in this work were obtained from Merck Inc.

2. Apparatus and Experimental Procedure

A schematic diagram of the experimental setup is illustrated in Fig. 1. The microreactor was fabricated from glass tubes with outer, inner diameters of 1 mm and 800 μm and lengths of 15, 25 and 35 cm. The microreactor was immersed in a container (with diameter of 9 cm and height of 11 cm) equipped with an ultrasound wave transducer to evaluate the effect of ultrasound waves on the

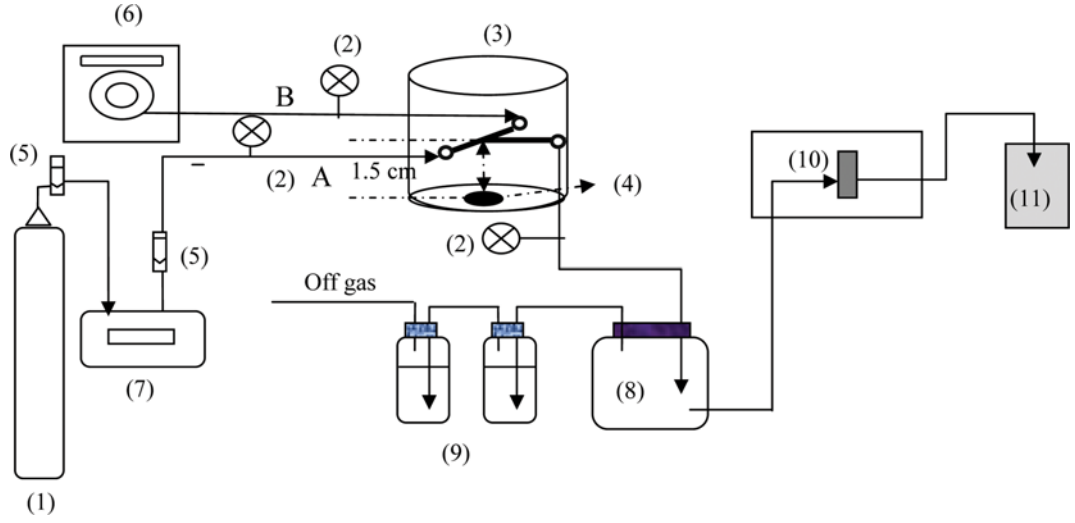

Fig. 1. A schematic diagram of the experimental setup.

(1) Oxygen cylinder
(2) Pressure sensor
(3) Microreactor
(4) Piezoelectric transducer
(5) Gas flow meter
(6) Peristaltic pump
(7) Ozone generator
(8) Phase separator
(9) Absorption bottles
(10) Spectrophotometer
(11) Product container

micromixing and also mass transfer rate performance inside the microreactor. A high frequency piezoelectric transducer (1.7 MHz, model ANN-2517GRL, Annon piezo technology Co. Ltd., China) with a diameter of 1.5 cm was installed at the bottom of the container. The transducer consumes electrical power around 9.5 W. In our previous study [26], the amount of actual energy dissipated ($P_{diss.}$) in the bulk of liquid (in the container) and in the microchannel was 8.526 (W) and 4.45×10^{-4} (W), respectively. Ozone was produced from pure oxygen by using an ozone generator (54520 LAXOU-France) with input rate of 1 g/h. The applied ozone dosage was controlled by a flow meter (LZB-3WB, China), which had a measuring range from 0-100 ml/min. The ozone stream from the ozone generator was introduced into the A channel and RB solution was introduced into the B channel from their liquid tanks by a peristaltic pump (Qis^{TM} DSP100). For gas and liquid separation, a two-phase mixture was diverted into a sealed phase separator, and the subsequently gas flowed into two absorption bottles filled with 2% (w/v) KI solution for ozone absorption. Liquid samples were collected from the microreactor output stream and the absorbance of the sample was measured at the maximum absorption wavelength of 554 nm. In all experiments, the measurements of samples continued until the value of decolorization efficiency reached a stable value. All experiments were conducted at 25±2 C°. The pressure drop was measured using two pressure transducers (BD sensor, DMP 343, Germany) installed at the inlet and outlet sides of the microreactor.

3. Analytical Methods

The samples' absorption was measured using a UV-spectrophotometer, manufactured by the UNIC Company, at the maximum absorbance wavelength of RB, which was 554 nm. A calibration curve was obtained based on evaluating the light absorption at various RB concentrations. Then, the decolorization efficiency was obtained by measuring the absorption intensity of the solution at 554 nm. The decolorization efficiency (%) of RB is defined as follows:

$$\text{Decolorization efficiency (\%)} = \left(1-\frac{C_i}{C_o}\right)\times 100 \quad (1)$$

C_o and C_i are concentration of RB in aqueous solution at the initial condition and the outlet stream, respectively. The outlet stream from the ozone generator contained an ozone-oxygen mixture. The unused ozone from the microreactor was diverted into two absorption bottles, which contained 2% KI solution. Potassium iodide solution reacted with unused ozone as shown in Eq. (2):

$$O_3+KI+H_2O\rightarrow I_2+2KOH+O_2 \quad (2)$$

The produced iodine was titrated using standard sodium thiosulfate, in the presence of starch as indicator [12,47]. The ozone concentrations in the gas stream at the microreactor inlet and outlet (unused) were measured using this method.

4. Experimental Design and Mathematical Model

The design of experiment (DOE) was used for optimization and process design. Response surface methodology (RSM) and central composite design (CCD) were applied to find the effect of each variable on RB removal efficiency. The five most important operating variables containing pH (A), RB concentration (B), flow rate RB (C), length of microreactor (D) and flow rate O_3 (E) were selected to find optimum conditions removal of RB and achieve to maximum removal yield. The ranges and levels of studied process variables are listed in Table 1. The percent of RB removal obtained from the reaction in presence and without ultrasonication was chosen as two outcome responses.

Table 1. Experimental range and levels of the independent variable

Variable	Factor code	Level and reactor range (coded)		
		−1	0	1
pH	A	3	6.5	10
Concentration of Rhodamine B (ppm)	B	50	65	80
Flow rate Rhodamine B (ml/min)	C	2	6	10
Length of microchannel (cm)	D	15	25	35
Flow rate O_3 (ml/min)	E	10	25	40

The mathematical model is presented by Eq. (3):

$$Y_{yield}=\beta_0+\sum_{i=1}^{3}\beta_{ii}X_i^2+\sum_{i=1}^{2}\sum_{j=i-1}^{3}\beta_{ij}X_{ij} \quad (3)$$

In which, Y_{yeild} is the removal efficiency, X_i and X_{ij} are the uncoded independent variables, β_0 is offset term and β_i, β_{ij}, β_{ii} are regression coefficients. A reliable method to analyze and define the degree of certainty of experimental data is analysis of variance (ANOVA) [48]. The response variable (removal efficiency) was fitted with quadratic regression model to relate the removal efficiency to these response variables. The coefficients of determination (R^2) and analysis of variance were used to evaluate the quality of the model. The levels and actual experimental design matrix is presented in Table 2.

RESULTS AND DISCUSSION

1. Determination of Ozone Mass Transfer Coefficient (k_La)

To define the effect of ultrasound wave irradiation on mass transfer coefficient in a microreactor, some experiments were carried out with and without sonication. With the help of a high-speed photography system, flow patterns were observed in microreactor. Flow patterns observed in the considered range are slug flow. Fig. 2 shows some representative images captured in the middle section of the microreactor at two flow rates. The reaction between ozone gas and dye solution was fast; therefore, the rate-controlling step was the mass transfer of ozone into the liquid phase, which is negligible due to the low solubility of ozone in solution [49-51]. Thus, with assumption of negligible rate of ozone self-decomposition, the average overall liquid mass transfer coefficient (k_La) can be derived by the following Eq. (4) [51,52]:

$$k_La=\frac{Q_L}{\pi R_i^2 L}\ln\left(\frac{C^*-C_{O_3,\,in}}{C^*-C_{O_3,\,out}}\right) \quad (4)$$

where Q_L is the liquid volumetric flow rate ($m^3\ s^{-1}$), L is the length of the microchannel of the (m), R_i is the radius of the inner tubes of the microreactor (m). $C_{O_3,\,in}$ and $C_{O_3,\,out}$ are the concentrations of dissolved ozone in the inlet and outlet of liquid phase (mol L^{-1}),

Table 2. Experimental conditions and results of central composite design

Run	A	B	C	D	E	Responses					
						Y1 (%)			Y2 (%)		
						Actual	Predicted	Error (%)	Actual	Predicted	Error (%)
1	6.5	65	6	25	25	61	60.875469	0.20415	65.5	65.11263	0.591412
2	6.5	65	2	25	25	78.2	79.249069	−1.34152	85.2	84.89207	0.361426
3	6.5	65	6	25	25	59	60.875469	−3.17876	65.9	65.11263	1.194803
4	3	80	10	35	10	44.7	46.388605	−3.77764	46.8	47.02278	−0.47603
5	10	50	2	35	10	80.2	83.622015	−4.26685	89.1	89.79473	−0.77972
6	10	80	2	35	40	87.7	86.371948	1.514312	92.3	89.48171	3.053402
7	3	50	10	15	40	55.4	54.221922	2.126495	60.12	57.71268	4.004192
8	10	80	10	35	10	39.11	39.553315	−1.13351	42.4	40.97569	3.359222
9	6.5	80	6	25	25	58.5	57.817839	1.166088	60.3	62.14503	−3.05974
10	6.5	65	6	25	25	59	60.875469	−3.17876	63.5	65.11263	−2.53957
11	6.5	65	10	25	25	43.5	42.501869	2.294555	49.3	45.33319	8.046278
12	3	50	10	35	40	62.3	61.369058	1.494289	66.4	65.23008	1.761928
13	6.5	65	6	15	25	59	59.297031	−0.50344	64.7	65.36493	−1.0277
14	10	50	2	15	10	70.3	70.487401	−0.26657	84.5	82.27733	2.630379
15	3	50	2	35	10	93.2	90.457305	2.942806	95.3	95.84182	−0.56854
16	10	50	10	35	10	47.1	46.903615	0.416954	49.2	46.91089	4.652663
17	3	80	10	35	40	53.7	54.018758	−0.59359	58.5	59.29488	−1.35877
18	6.5	65	6	25	25	63	60.875469	3.372272	68.1	65.11263	4.386747
19	10	50	10	15	40	48.35	47.386632	1.992488	52.11	51.66559	0.852831
20	10	65	6	25	25	55.7	57.457824	−3.15588	59.4	62.08908	−4.52707
21	6.5	65	6	35	25	72.1	69.437906	3.692224	75.3	72.88233	3.210724
22	3	80	2	15	40	82.5	83.647622	−1.39106	88.3	88.0114	0.32684
23	6.5	65	6	25	40	66.7	65.584295	1.672721	68.3	69.5862	−1.88316
24	3	50	10	35	10	53.2	53.738905	−1.01298	56	52.95798	5.432179
25	6.5	65	6	25	25	59.9	60.875469	−1.6285	64.7	65.11263	−0.63775
26	10	80	10	35	40	49.2	47.183468	4.098642	52.3	53.24779	−1.81222
27	10	80	10	15	10	30	28.831181	3.896065	32.5	33.45829	−2.94858
28	3	80	10	15	40	46.12	46.871622	−1.62971	51.2	51.77748	−1.12789
29	3	80	2	35	40	92.1	93.207238	−1.20221	96.2	95.5288	0.697713
30	6.5	65	6	25	10	56.5	56.166643	0.590013	59.4	60.63906	−2.08595
31	3	50	2	35	40	96.7	98.087458	−1.43481	98.2	101.464	−3.32383
32	3	50	2	15	10	80.4	77.322691	3.827499	86.2	88.32442	−2.46452
33	10	50	2	35	40	90.3	91.252168	−1.05445	93.7	95.41691	−1.83235
34	10	80	10	15	40	40.8	40.036332	1.871735	46.2	45.73039	1.016472
35	6.5	50	6	25	25	66.13	63.933099	3.322095	70.4	68.08023	3.295135
36	3	50	10	15	10	40.2	43.016771	−7.00689	42.2	45.44058	−7.6791
37	10	50	2	15	40	83.2	81.692552	1.811837	90	87.89951	2.333878
38	6.5	65	6	25	25	60.58	60.875469	−0.48773	65.11	65.11263	−0.00403
39	10	80	2	35	10	79	78.741795	0.326842	82.1	83.85953	−2.14315
40	6.5	65	6	25	25	61.33	60.875469	0.741124	64	65.11263	−1.73848
41	6.5	65	6	25	25	60.5	60.875469	−0.62061	65.3	65.11263	0.286945
42	10	80	2	15	40	76.1	76.812332	−0.93605	82.1	81.96431	0.165274
43	10	50	10	35	40	52.5	54.533768	−3.87384	55.7	59.18299	−6.25312
44	3	50	2	15	40	86.7	88.527842	−2.10824	93.4	93.9466	−0.58522
45	3	65	6	25	25	64.5	64.293114	0.320754	67.4	68.13617	−1.09224
46	3	80	2	15	10	73.7	72.442471	1.706282	87.4	82.38922	5.733158
47	10	80	2	15	10	64.3	65.607181	−2.03294	75.13	76.34213	−1.61338
48	10	50	10	15	10	36.8	36.181481	1.68076	38.4	39.39349	−2.58721
49	3	80	10	15	10	34.2	35.666471	−4.28793	36.8	39.50538	−7.35158
50	3	80	2	35	10	87.3	85.577085	1.973557	89.5	89.90662	−0.45432

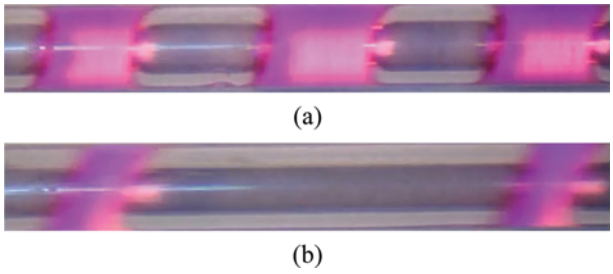

Fig. 2. Representative photographs of ozone-dye solution flow pattern in the microreactor. Pictures were captured in the middle section of the microreactor: (a) Q_G=10 ml/min, Q_L=2 ml/min; (b) Q_G=40 ml/min, Q_L=2 ml/min.

respectively. The value of C^*, equilibrium ozone concentration, was calculated by Henry's Law constant as follows:

$$C^* \text{ (mol/L)} = 55.56 P_{O_3}/H \quad (5)$$

In addition, H is Henry's Law constant, which could be obtained by Eq. (6) [49,53]:

$$H(\text{atm/L/mol}) = 3.84\times10^7 (10^{pH-14}) \exp\left(-\frac{2428}{T}\right) \quad (6)$$

The measured k_La for decolorization process of both modes in different length of microreactor and ozone gas flow rate are shown in Table 3. It can be clearly seen that for a fixed length of microreactor, k_La increased significantly with increase of Q_G, while k_La decreased with increase in the length of microchannel at a constant Q_G. With increase in both parameters, the ozone mass transfer (absorbed ozone in liquid) increases in the microreactor. The effect of Q_G on the increase of k_La can be due to increase of more local turbulence and the reduction of thickness liquid boundary layer, thereby mass transfer resistance decreases and k_La of microreactor increases. However, contact time of two phases increases with an increase of microreactor length, but the value of k_La has decreased. This can be due to reduction of driving force, which leads to reduction of mass transfer rate along the microreactor.

Table 3. Mass transfer coefficients in microreactor with and without activated PZT

$Q_{ozone\text{-}gas}$ (ml/min)	Length of microchannel (cm)	k_La, with US (min^{-1})	k_La, without US (min^{-1})
10	15	6.47	3.38
40	15	7.382	4.1
10	35	0.767	0.622
40	35	0.933	0.884

It is also evident that ultrasound wave irradiation during the microreactor has a significant effect on the k_La compared with the plain microreactor. These results are due to the strong micro streams and local turbulence induced by the collapse of microbubbles, generated by the high frequency wave propagation. These phenomena can enhance effectively the solution mixing and more contact of between ozone and dye solution, which can increase the mass transfer coefficient as well as the decolorization efficiency of dye solution. In the following sections, the effect of various parameters on the application of ultrasound wave for the removal of dyes from solution in the microreactor was investigated.

Table 4. Analysis of variance table for response surface reduced quadratic model

Responses	Model terms	Sum of square	Mean square	F value	Prob>F
Y1	Model	14125.86	1569.54	589.23	<0.0001
	A	411.267	411.267	154.396	<0.0001
	B	305.7	305.7	114.764	<0.0001
	C	11553.4	11553.4	4337.321	<0.0001
	D	894.11	894.11	335.64	<0.0001
	E	773.31	773.31	290.313	<0.0001
	BC	14.78	14.78	5.55	0.0235
	CD	14.24	14.24	5.35	0.0260
	DE	22.03	22.03	8.27	0.0064
	D^2	137.1	137.1	51.46	<0.0001
	Residual	106.55	2.6637		
	Lack of fit	94.505	2.86	1.67	0.2493 not significant
Y2	Model	15336.2	2190.89	510.29	<0.0001
	A	310.82	310.82	72.39	<0.0001
	B	299.44	299.44	69.74	<0.0001
	C	13301.65	13301.65	3098.15	<0.0001
	D	480.38	480.38	111.89	<0.0001
	E	680.42	680.42	158.48	<0.0001
	CE	88.44	88.44	20.6	<0.0001
	D^2	175.04	175.04	40.77	<0.0001
	Residual	180.32	4.29		
	Lack of fit	166.76	4.76	2.46	0.1082 not significant

2. Statistical Analysis and Model Development

A second-order polynomial equation was developed using the CCD to verify the factor interactions and optimize the considered parameters. The analysis of variance (ANOVA) for two responses (Y_1 and Y_2) is given in Table 4. The quadratic regression model was selected to predict the yield of removal RB.

3. Response Surface Modeling

The model for removal efficiency of RB in the plain microreactor in terms of coded factors is expressed by Eq. (7).

$$\text{The removal efficiency (\%), } Y_1 \text{ (coded factors)} = 60.88 - 3.48A - 3B - 18.43C + 5.13D + 4.77E - 0.68BC - 0.67CD - 0.83DE + 3.55D^2 \quad (7)$$

The model F value, which the model equation was evaluated by it, indicates that the model is significant at 95% confidence level. The value of regression coefficient R^2 and the adjusted coefficient (R^2 adj.) were 99.25% and 99.08%, respectively. The high value determination coefficient (R^2) represented a good fitness between model and experimental results and demonstrated that the model was reliable for removal efficiency of RB. In this case A, B, C, D, E, BC, CD, DE and D^2 are significant model terms. Other model terms with a p-value larger than 0.05 were eliminated. Moreover, the quadratic equations of removal efficiency of RB in combined microreactor with ultrasound waves are given below:

The Removal efficiency (%) of the sonicated microreactor, Y_2 (coded factors) is equal to:

$$65.11 - 3.02A - 2.97B - 19.78C + 3.76D + 4.47E + 1.66CE + 4.01D^2 \quad (8)$$

The statistical significance of the above equation was the controlled F-value. The p-value lower than 0.05 was chosen and shows model terms are significant. The correlation coefficient (R^2=98.84%) and adjusted R-squared (R_{adj}^2=98.64%) as a measure of model fit demonstrate good agreement between the experimental result and the predicted values. In this model, the terms A, B, C, D, E, CE, D^2 were significant.

4. Effect of Process Parameters on Removal Efficiency of RB (%)

All of experiments were carried out in two approaches, with and without activated transducer. Influence of both modes on the operating conditions was studied.

4-1. Effect of pH on RB Removal Efficiency

The parameter of pH plays an effective role in the ozone oxidation process [49]. In the reported studies in literature [44,50], the dye removal efficiency is dependent on direct oxidation by ozone and radical oxidation by $OH^{\bullet}$ in solution. On other hand, direct oxidation is more selective in comparison with radical oxidation and dominates under low pH conditions [10]. Fig. 3 illustrates the effect of pH on the removal efficiency of RB. From these results, it can be seen that an increase in pH from 3 to 10 results in a decrease in removal of RB for both modes. These reductions in efficiency are from 67.4% to 59.4% for the microreactor with ultrasound wave irradiation and from 64.5% to 55.7% for the plain microreactor. These can be due to decolorization rate in acid condition, which is better than that of in alkali condition with free radical scavengers due to high solution pH. Consequently, the removal rate of RB decreased with reduction of $OH^{\bullet}$ radical concentration in solution. Fig. 3 also shows that removal efficiency of RB in the sonicated

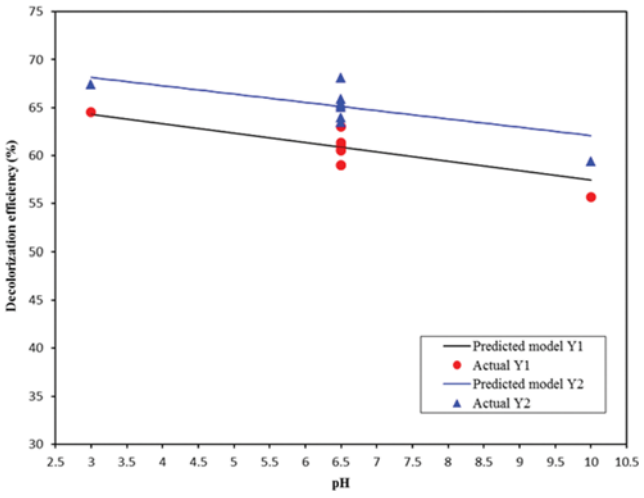

Fig. 3. The effect of pH on the dye decolorization of Rhodamine B for both of modes. C_{RB}=65 mg/L, $Q_{ozone\,gas}$=25 ml/min, Q_{RB}= 6 ml/min, length of microreactor=25 cm.

microreactor is higher than the plain microreactor at the same time. This result is due to the enhanced micromixing in the liquid slug with high frequency wave propagation, which increases the interfacial area between two phases [27]. Moreover, the ultrasound wave propagation can be effective on the slug size and improve internal circulation within these slugs [54].

This phenomenon has a significant effect on ozone mass transfer rate from gas phase into gas-liquid interface, which results in more direct oxidation and more generated concentration of $OH^{\bullet}$ radicals.

4-2. Effect of Initial Concentration on RB Removal Efficiency

The effect of dye concentration on the decolorization efficiency was investigated in the range from 50 to 80 mg/L. Fig. 4 indicates that the removal rate of RB declined with an increase in the dye concentration for both modes. This can be explained by the fact

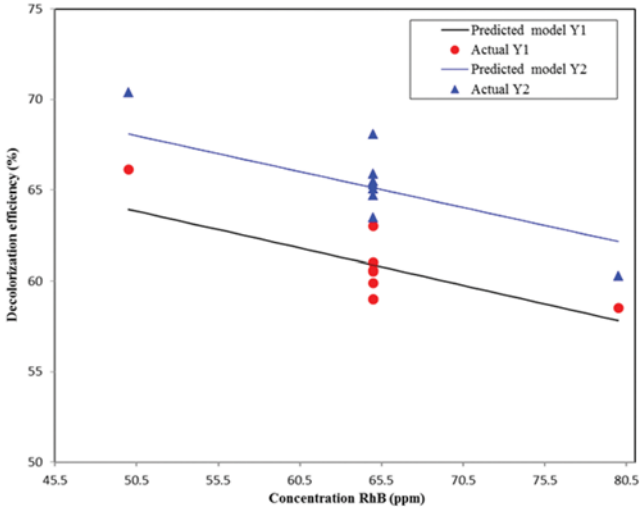

Fig. 4. The effect of initial concentration RB on the decolorization efficiency of dye for both of modes. pH=6.5, $Q_{ozone\,gas}$=25 ml/min, $Q_{L,RB}$=6 ml/min, length of microreactor=25 cm.

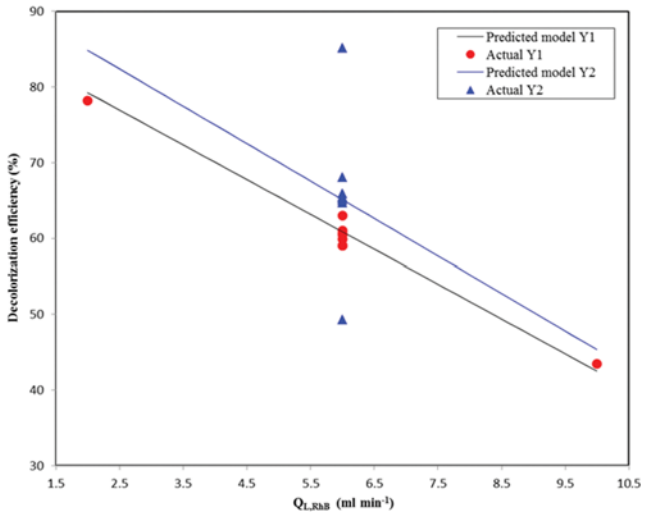

Fig. 5. The effect of liquid volumetric flow rate of RB on the decolorization efficiency of dye for both of modes. pH=6.5, $Q_{ozone\,gas}$ =25 ml/min, C_{RB}=65 mg/L, length of microreactor=25 cm.

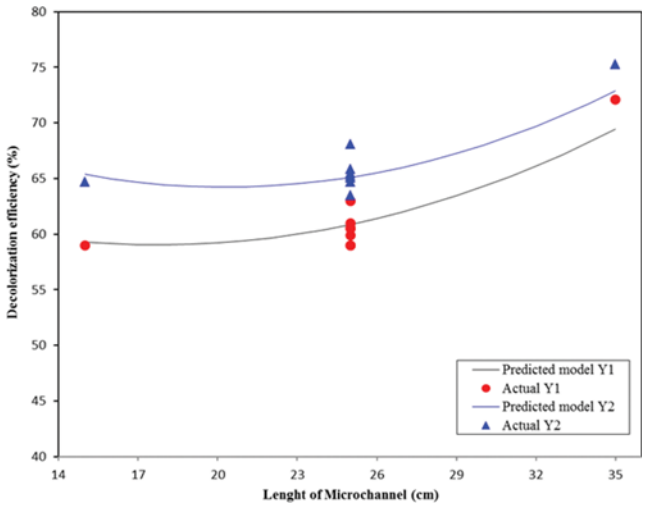

Fig. 6. The effect of length of microreactor on the decolorization efficiency of dye for both of modes. pH=6.5, $Q_{ozone\,gas}$=25 ml/min, C_{RB}=65 mg/L, $Q_{L,RB}$=6 ml/min.

that with increasing RB concentration at the same condition, there are more RB molecules in the solution. Therefore, with constant number of generated hydroxyl radicals in the solution, the removal efficiency decreased. On the other hand, the efficiency performance of sonicated microreactor is more than that of the plain microreactor at various dye concentrations. The mixing enhancement by ultrasound waves increases the ozone solubility and its mass transfer rate into gas-liquid interface. Therefore, higher decolorization efficiency was achieved in the sonicated microreactor.

4-3. Effect of Flow Rate of RB Removal Efficiency

In this part, the effect of liquid volumetric flow rate on the removal efficiency was examined. Fig. 5 represents the relationship between the decolorization efficiency and flow rate of RB. The decolorization efficiency decreased with an increase in liquid volumetric flow rate from 2 to 10 ml/min in the two examined layouts. This might be due to reduction of contact time between ozone and dye solution, which leads to decrease in decolorization efficiency. By referring to this figure, one can see that by ultrasound wave propagation in all studied flow rate, decolorization efficiency values increased. However, the effect of sonication was more significant at lower flow rates. This might indicate that at lower flow rates the ultrasound waves has a more significant effect on micromixing performance. This is due to variety of mechanical effects due to explosion of microbubbles, which enhances the interaction between ozone and dye solution.

4-4. Effect of Microreactor Length

Fig. 6 displays the effect of various length of microreactor on the dye removal efficiency. As shown, the decolorization efficiency was significantly influenced by the microreactor length. This can be due to increase in interaction time between ozone and Rhodamine B solution, and thereby a better gas-liquid mass transfer. In addition, the results demonstrate that the sonicated microreactor was more successful in RB removal in comparison with the plain microreactor. For example, the decolorization efficiency by sonication has improved about 12% in the length of 15 cm and 5.5% in the length of 35 cm. One can notice that the better performance of the sonicated microreactor can be due to stronger induced micro-streams and micro-jets. These phenomena have a positive effect on micromixing performance and can enhance the rate of mass transfer, and thereby an increase in decolorization efficiency [27].

4-5. Effect of Ozone Flow Rate RB Removal Efficiency

It is clear that an increase in ozone flow rate can enhance the local turbulence and therefore gas-liquid mass transfer rate due to higher contact surface. In this part, the effect of ozone flow rate changes (in the range of 10-40 ml/min) in a constant Q_L (6 ml/min) on RB removal efficiency is investigated. From the results shown in Fig. 7, it is clear that the decolorization efficiency of RB with the increase of the ozone gas flow rate was enhanced for both modes. With an increase in O_3 concentration in the liquid phase, the amount

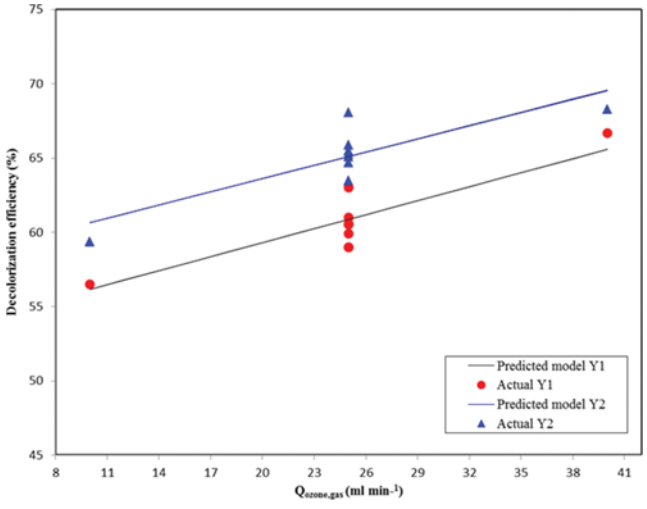

Fig. 7. The effect of ozone gas volumetric flow rate on the decolorization efficiency of dye for both of modes. pH=6.5, length of microreactorl=25 cm, C_{RB}=65 mg/L, $Q_{L,RB}$=6 ml/min.

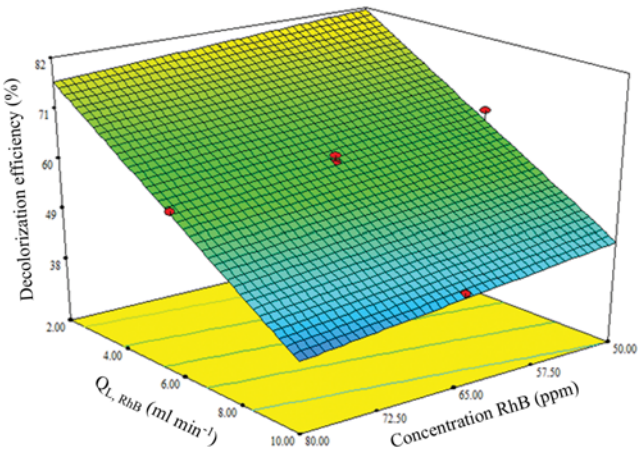

Fig. 8. Response surface plot for decolorization efficiency (%) with respect to $Q_{L,RB}$ (ml min^{-1}) and C_{RB} (ppm) at constant values of pH=6.5, C_{RB}=65 mg/L, $Q_{ozone,gas}$=25 ml min^{-1}, length of microreactor=25 cm.

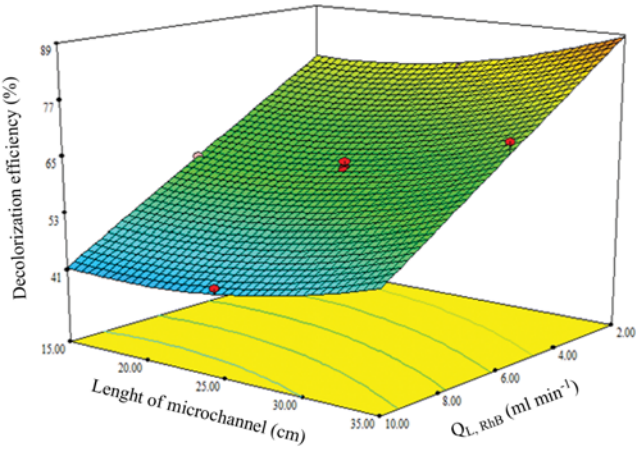

Fig. 9. Response surface plot for decolorization efficiency (%) with respect to $Q_{L,RB}$ (ml min^{-1}) and length of microreactor (cm) at constant values of pH=6.5, C_{RB}=65 mg/L, $Q_{ozone,gas}$=25 ml/min.

of generated $OH^{\bullet}$ radicals in the system increased, which can enhance the decolorization of RB. On the other hand, as shown in this figure, increase of decolorization efficiency was obtained for all the ozone flow rates by ultrasound irradiation. This result is due to the strong micro-streams and micro-jets induced by the collapse of microbubbles, generated by the high frequency wave propagation. These phenomena have significant effects on enhancing of the solution mixing. A more efficient mixing caused a considerable reduction in gas-liquid mass transfer resistance and consequently an increase in O_3 concentration in the liquid phase, which is effective for decolorization of the solution.

5. Interaction Between Process Variables

The three-dimensional response surface was plotted to investigate interaction and effect of the five process variables on decolorization efficiency of RB. Fig. 8 indicates the influence of initial concentration and flow rate of RB on decolorization efficiency in the plain microreactor. It can be seen that decolorization efficiency in entire range of Rhodamine B solution flow rate was reduced with increase in the RB concentrations. In addition, increase in flow rate of RB has undesirable effect on the removal efficiency at different RB concentrations. The contour plot reveals that these two parameters have significant negative effect on the decolorization efficiency of RB. An increase in the RB flow rate from 2 to 10 ml/min caused a reduction of 43.5% and 49.4% in decolorization efficiency for concentration of 50 ppm and 80 ppm, respectively. However, with the concentration changes of RB from 50 to 80 ppm in RB flow rate 2 ml/min, the RB removal decreased about 5.8% in RB flow rate of 10 ml/min and 15.6% in flow rate of 40 ml/min. From the obtained results, it seems that the change in RB flow rate had a significant effect on decolorization efficiency as compared with the initial change of RB concentration. This can be because the RB flow rate has a higher coefficient value than RB concentration. With an increase in RB flow rate at a constant Q_G, the contact time between two phases and also ozone dose per volume of dye solution and thereby decolorization efficiency were reduced in the microreactor. Fig. 9 shows the effect of interaction between length of microreactor and RB flow rate. An increase in these variables leads to two opposite effects. Increase in the flow rate of RB from 2 to 10 ml/min caused a reduction of 46.17% and 43.1% in decolorization efficiency for the length of 15 cm and 35 cm, respectively. On the other hand, with an increase in the length of microreactor from 15 to 35 cm in RB flow rates of 2 and 10 ml/min, decolorization efficiency increased 12.8% and 17.8%, respectively. This can be the result of increase in flow rate, which has negative effect on the yield of RB decolorization due to reduction in contact time between two phases. However, increase in length of microreactor has a positive effect on it due to increase in interaction time and driving force for the transfer of ozone to the dye solution. Fig. 10 shows the interaction effect of length of microreactor and ozone flow rate. The results clearly indicate that both of the variables have positive effect on RB removal rate. With an increase in these variables, the removal rates increased. The results show that at higher ozone volumetric flow rate and length of microchannel, ozone mass transfer rate and

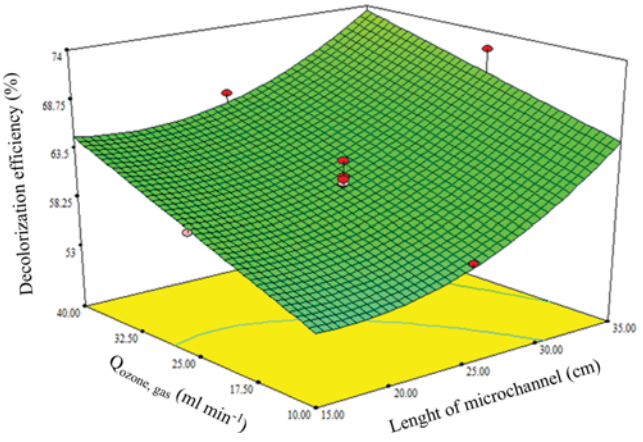

Fig. 10. Response surface plot for decolorization efficiency (%) with respect to $Q_{ozone,gas}$ (ml min^{-1}) and length of microreactor (cm) at constant values of pH=6.5, C_{RB}=65 mg/L, $Q_{L,RB}$=6 ml min^{-1}.

thereby ozone concentration in the liquid phase increased. With increasing the length of microreactor at a fixed Q_G, due to increase in contact time in the system, decolorization efficiency of RB in the microreactor was increased. On the other hand, with increasing the value of Q_G at a fixed microreactor length, the residence time and contact time between two phases decreased. It is mainly attributed to the fact that the increase of Q_G can increase the local turbulence and subsequently cause thinner thickness of liquid boundary layer, which results in the reduction of mass transfer resistance between the gas-liquid phases. This can cause an increase in mass transfer rate. In addition, according to the presented model by design of experiment for sonicated microreactor, interaction between O_3 flow rate and RB flow rate was found. The interaction effect of the two variables, namely ozone flow rate and RB flow rate on removal efficiency of RB, is shown in Fig. 11. This figure illustrates that an increase in the ozone flow rate improved the RB removal efficiency. For example, at RB flow rate of 10 ml/min, RB removal 23.5% increased when ozone volumetric flow rate enhanced from 10 to 40 ml/min. This can be due to higher gas holdup and turbulence intensity inside the microreactor, which can cause more contact between the two phases and thereby increase in mass transfer rate. On the contrary, with an increase in the RB flow rate from 2 to 10 ml/min, the RB removal decreased 52.4% in ozone flow rate of 10 ml/min and 41.8% in ozone flow rate of 40 ml/min. It is clear that an increase in the flow rate RB variable has a negative significant effect on decolorization efficiency, which reduces contact time between two phases and also ozone dose per volume of dye solution at a high RB flow rate. Moreover, it was found that RB flow rate indicated more linear effect (higher coefficient values) on the removal rate for both reactors with and without sonication.

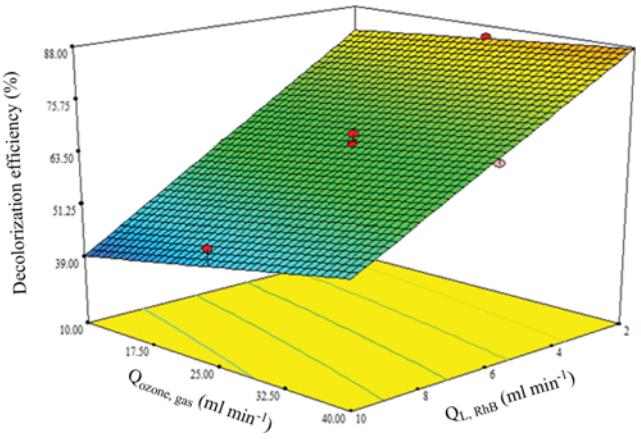

Fig. 11. Response surface plot for decolorization efficiency (%) with respect to $Q_{L,RB}$ (ml min^{-1}) and $Q_{ozone,gas}$ (ml min^{-1}) at constant values of pH=6.5, length of microreactor=25 cm, C_{RB}= 65 mg/L.

6. Process Optimization Using Response Surface Methodology

In the present study, a numerical optimization technique was performed based on the presented models (Eqs. (7) and (8)) to determine the optimum conditions to reach a higher yield of Rhodamine B removal. To provide an ideal case for decolorization efficiency for both systems, input variables were set in range. The value of the responses (Y_1 and Y_2) was set at maximum values.

The optimal values of input process parameters are given in Table 5. An additional two experiments were conducted to verify the accuracy of presented optimum conditions by the experimental design method for both reactors with and without sonication. Table 5 shows the predicted values of decolorization efficiency derived from the regression equations as well as the experimental results obtained by the optimal setting of the parameters. The predicted responses were found to be in good agreement with the experimental results with an error of <±1% for both modes. In addition, for better comparison between the predicted values by model and the experimental results, a new experiment was performed in condition of removal efficiency about of 60% for both modes (Table 6). The result indicated a good agreement between the experimental results with the model predictions, which confirms the reliability of the regression model for both modes.

7. Energy Efficiency

As illustrated above, using high frequency piezoelectric transducer, due to the intense mixing through microreactor and enhanced interaction between ozone gas and Rhodamine B solution, is an efficient way to remove RB from wastewater. However, using ultrasound waves in a microreactor can increase the pressure drop across the reactor and the amount of energy consumption. Therefore, the pressure drop across the microreactor can be used to evaluate the mixing performance per energy consumption in the studied microreactors. For this purpose, the pressure drop across the channels during the decolorization efficiency was measured at various feed flow rates. Fig. 12 shows the pressure drop values in the microreactor in presence of and without ultrasound irradiation at various flow rates for 25 cm length. The experimental results reveal that ultrasound waves have caused a very low difference in pressure

Table 5. Optimized input process parameters and optimum value of Decolorization efficiency

Responses	Solution	A	B	C	D	E	Predicted value (%)	Experimental value (%)	Error (%)
Y1	1	3.02	50	2	35	36.91	96.46	95.8	−0.7
Y2	1	3	57.48	2	35	30.5	98.21	97.3	−0.941

Table 6. Input process parameters and value of Decolorization efficiency

Responses	Solution	A	B	C	D	E	Predicted value (%)	Experimental value (%)	Error (%)
Y1	1	3	50	10	35	40	63.15	62.3	−1.36
Y2	1	3	50	10	35	40	67.03	66.4	−0.95

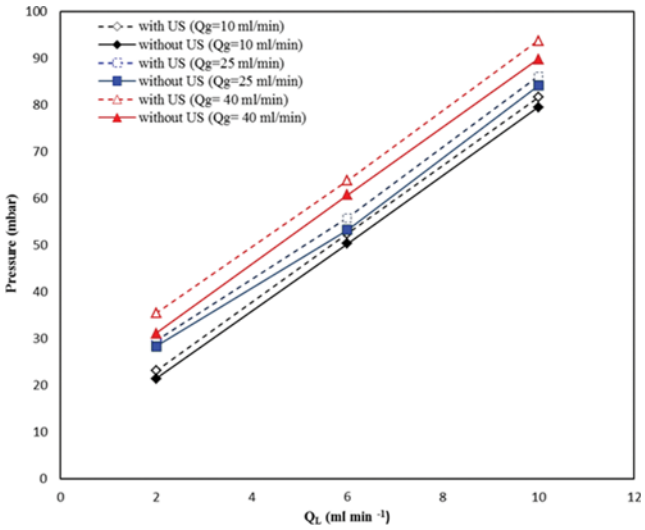

Fig. 12. Pressure drop at various flow rates in microreactor: L=25 cm.

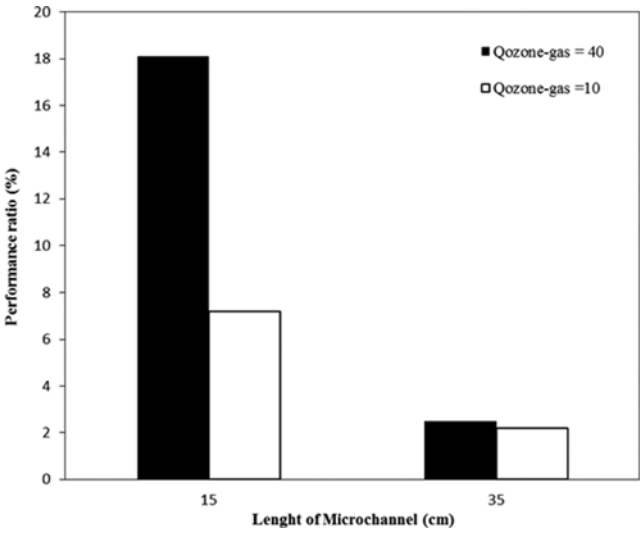

Fig. 13. The performance ratios for different lengths of microreactor at the various flow rates of $Q_{ozone\,gas}$. Length of microreactor=25 cm, $Q_{L,RB}$=2 ml min^{-1}, C_{RB}=80 mg/L, pH=3.

drop across the microreactor. However, ultrasound waves have a significant impact on the decolorization performance of dye from solution (more explanation was presented in the previous sections).

Moreover, the performance ratio, which was previously presented for heat transfer purposes [48], is defined using the decolorization efficiency of RB (Y) and friction factor based on with and without the presence of ultrasound irradiation in the microreactor as follows [27,50]:

$$\text{Performance ratio} = \frac{\frac{Y_2}{Y_1}}{\left(\frac{f_2}{f_1}\right)^{1/3}} \tag{9}$$

and

$$f = \frac{\Delta P}{(L/D)(\rho u^2/2)} \tag{10}$$

In which, Y_2, f_2 are the removal efficiency of RB and friction factor when the microreactor is equipped with a piezoelectric transducer and Y_1, f_1 are the removal efficiency of RB and friction factor when the piezoelectric transducer is inactivated in the microreactor. The calculated performance ratios for different lengths of microreactor at the various flow rates are illustrated in Fig. 13. The performance ratios of combined microreactor with ultrasound wave are increased with reduction in flow rate (the sum of flows of ozone gas and liquid) and length of microreactor. This may be because at lower feed flow rate and length of channel, the role of ultrasound wave in increasing mixing intensity and ozone transfer into the solution is more significant. In other words, at higher flow rates the macromixing and convective flow circulation and also at higher length of microreactor the increase of contact time for two phases are more significant than extra mixing and interaction between gas-liquid phases by ultrasound waves.

8. Comparison with Other Gas-liquid Contactors

The liquid side mass transfer coefficient of the microreactor for both modes with and without the presence of irradiation of ultrasound wave was compared with other conventional gas-liquid contactors. Although the experimental conditions were different, it can be inferred from Table 7 that the k_La value of T-type microreactor with least energy consumption is higher than water-jacketed glass reactor presented by Weavers [32]. As previously mentioned, k_La value increases significantly with increasing in Q_L and Q_G. However, the difference is very high between volumetric flow rate of microporous tube-in-tube microreactor presented by Gao [26] and micro reactor equipped with ultrasonic waves in this work. However, the mass transfer coefficient in sonicated microreactor is very near to the microporous tube-in-tube microreactor [26]. This could mean that the sonicated microreactor is a very good gas-liquid contactor for enhancing mass transfer due to the variety of mechanical effects that increase local turbulence besides the microstream

Table 7. k_La Obtained in T-type of microchannel and conventional reactors

Type of contactor	Frequency	Q_G (ml/min)	Q_L (ml/min)	k_La (min^{-1})	P_{diss} (W/L)
Microporous tube-in-tube microreactor [26]	----	666.6-1333.3	200-400	2.5-8.23	---
Water-jacketed glass reactor [32]	20 kHz	10-40	---	0.025-0.15	263
	500 MHz	10-40	---	0.012-0.05	50.3
T-type (without ultrasound)	1.7 MHz	10-40	2	0.622-4.1	---
T-type (with ultrasound)	1.7 MHz	10-40	2	0.767-7.5	0.03-0.06

propagation.

CONCLUSIONS

A T-shaped microreactor equipped with a high frequency (1.7 MHz) transducer was used to enhance the mass transfer rate and removal efficiency of RB. Ultrasound waves in this range are able to improve micromixing and mass transfer rate. The main aim of this study was to evaluate the effect of ultrasound wave irradiation in a microreactor involved with two-phase flow RB decolorization. The measured results show that the decolorization efficiency increased with increase of ozone gas volumetric flow rate, while decreased with increase of RB initial concentration and liquid volumetric flow rate. The results illustrate that increase in length of the microreactor led to increase in decolorization efficiency. In addition, the decolorization rate was more in acidic medium, at pH of 3, due to the combined action of ozone and hydroxyl radicals. Overall, the ultrasound irradiation in a microreactor has significant effect on the RB removal efficiency compared with the plain microreactor. To achieve the highest decolorization efficiency of RB in a microreactor, response surface methodology experimental analysis technique was used. The results show that at optimum conditions, decolorization efficiency of 97.3% can be obtained by employing high frequency ultrasound wave irradiation. For more analysis, performance ratio of ultrasound wave propagation in microreactor in comparison with plain one was studied, and the results indicated a significant impact of ultrasound irradiation at various gas flow rates and microreactor lengths. Finally, the effect of ultrasound wave on mass transfer rate coefficient (k_La) was investigated. The results showed the desired effect of ultrasound wave on mass transfer rate coefficient. This phenomenon was explained by the fact that by using of ultrasound waves the micromixing and local turbulence intensity increase due to collapse of cavitation bubbles. Finally, it can be concluded that ultrasound wave irradiation in a microreactor has a great effect on mass transfer rate. This study suggests a new technique with high decolorization efficiency for wastewater treatment in comparison with other conventional methods.

NOMENCLATURE

L : main microchannel length [m]
R_i : microchannel radius [m]
Q_G : gas phase volumetric flow rate [m^3/s]
Q_L : liquid phase volumetric flow rate [m^3/s]
V : volume of main microchannel [m^3]
$C_{O_3,in}$: concentrations of dissolved ozone in the inlet liquid phase [mol L^{-1}]
$C_{O_3,out}$: concentrations of dissolved ozone in the outlet liquid phase [mol L^{-1}]
P_{O_3} : partial pressure in the gas phase [atm]
He_{O_3} : Henry's constant of O_3 kmol/[m^3/atm]
T : temperature [K]
C^* : equilibrium concentration of O_3 in the gas-liquid interface [mol/L]
A : light absorption
ΔP : pressure drop difference [atm]
C_0 : concentration of RB of solution at the initial condition [ppm]
C_i : concentration of RB of solution at the outlet stream [ppm]
u : fluid Velocity [m/s]

Greek Letters

β_0 : offset term, Eq. (3)
X_i, X_{ij} : uncoded independent variables
β_i, β_{ij}, β_{ii} : regression coefficients
f : friction factor
ρ : liquid density [kg/m^3]

Subscripts

In : microchannel inlet
out : microchannel outlet

REFERENCES

1. Y. Jin, Y. Wu, J. Cao and Y. Wu, *Korean J. Chem. Eng.*, **45**, 589 (2014).
2. S. Şahinkaya, *J. Ind. Eng. Chem.*, **19**, 601 (2013).
3. Y. Na, S. Song and Y. Park, *Korean J. Chem. Eng.*, **22**, 196 (2005).
4. Y.-S. Na, D.-H. Kim, C.-H. Lee, S.-W. Lee, Y.-S. Park, Y.-K. Oh, S.-H. Park and S.-K. Song, *Korean J. Chem. Eng.*, **21**, 430 (2004).
5. J. B. Parsa and F. N. Chianeh, *Korean J. Chem. Eng.*, **29**, 1585 (2012).
6. P. Ghosh, L. K. Thakur, A. N. Samanta and S. Ray, *Korean J. Chem. Eng.*, **29**, 1203 (2012).
7. A. Maleki, A. H. Mahvi, R. Ebrahimi and Y. Zandsalimi, *Korean J. Chem. Eng.*, **27**, 1805 (2010).
8. P. R. Gogate, M. Sivakumar and A. B. Pandit, *Sep. Purif. Technol.*, **34**, 13 (2004).
9. J. W. Choi, H. K. Song, W. Lee, K. K. Koo, C. Han and B. K. Na, *Korean J. Chem. Eng.*, **27**, 1805 (2010).
10. B. Cuiping, X. Xianfeng, G. Wenqi, F. Dexin, X. Mo, G. Zhongxue and X. Nian, *Desalination*, **278**, 84 (2011).
11. CH . Wu, *Dyes and Pigments*, **77**, 24 (2008).
12. K. Turhan and Z. Turgut, *Desalination*, **242**, 256 (2009).
13. A. D. Shah, N. Dai and W. A. Mitch, *Environ. Sci. Technol.*, **47**, 2799 (2013).
14. M. Tokumura, T. Katoh, H. Ohata and Y. Kawase, *Ind. Eng. Chem. Res.*, **48**, 7965 (2009).
15. J. Wu, H. Doan and S. Upreti, *Chem. Eng. J.*, **142**, 156 (2008).
16. L. B. Chu, X. H. Xing, A. F. Yu, , Y. N. Zhou, X. L. Sun and L. B. Jurcik, *Chemosphere*, **68**, 1854 (2007).
17. L. Kovalova, H. Siegrist, U. V. Gunten, J. Eugster, M. Hagenbuch, A. Wittmer, R. Moser and C. S. McArdell, *Environ. Sci. Technol.*, **47**, 7899 (2013).
18. K. Jahnisch, V. Hessel, H. Lowe and M. Baerns, *Chem. Int. Ed.*, **43**, 406 (2004).
19. W. Ehrfeld, V. Hessel and H. Lowe, Wiley-VCH, Weinheim (2000).
20. S. Ferrouillat, P. Tochon and H. Peerhossaini, *Chem. Eng. Process.*, **45**, 633 (2006).
21. P. Valeh-e-Sheyda, M. Rahimi, A. Parsamoghadam and H. Adibi, *JTICE*, **46**, 65 (2015).
22. M. Kashid, A. Renken and L. Kiwi-Minsker, *Chem. Eng. J.*, **167**, 436 (2011).
23. M. Rahimi, B. Aghel, M. Sadeghi and M. Ahmadi, *Desal Water*

Treat., **52**, 5513 (2014).
24. Y. Matsushita, N. Ohba, S. H. Kumada, K. Sakeda, T. Suzuki and T. Ichimura, *Chem. Eng. J*., **135**, 303 (2008).
25. J. R. Burns and C. Ramshaw, *Trans IChemE*, **77**, 206 (1999).
26. M. Gao, Z. Zeng, B. Sun, H. Zou, J. Chen and L. Shao, *Chemosphere*, **89**, 190 (2012).
27. M. Faryadi, M. Rahimi, S. Safari and N. Moradi, *Chem. Eng. Process.*, **77**, 13 (2014).
28. H. Monnier, A. M. Wilhelm and H. Delmas, *Chem. Eng. Sci*., **54**, 2953 (1999).
29. B. A. Bhanvase, D. V. Pinjari, S. H. Sonawane, P. R. Gogate and A. B. Pandit, *Ultrason Sonochem*., **19**, 97 (2012).
30. B. Pohl, R. Jamshidi, G. Brenner and U. A. Peuker, *Chem. Eng. Sci*., **69**, 365 (2012).
31. H. Monnier, A. M. Wilhelm and H. Delmas, *Chem. Eng. Sci*., **55**, 4009 (2000).
32. L. Weavers and M. Hoffmann, *Environ. Sci. Technol*., **32**, 3941 (1998).
33. X. K. Wang, J. G. Wang, P. Q. Guo, W. L Guo and C. Wang, *J. Hazard. Mater*., **169**, 486 (2009).
34. S. H. Chang, K. S. Wang, H. C. Li, M. Y. Wey and J. D. Chou, *J. Hazard. Mater.*, **172**, 1131 (2009).
35. A. Kumar, M. Paliwal, R. Ameta and S. Ameta, *Indian J. Chem. Technol*., **15**, 7 (2008).
36. V. K. Garg, R. Gupta and T. Juneja, *Chem. Biochem. Eng*., **19**, 75 (2005).
37. M. D. C. Cotto-Maldonado, T. Campo, E. Elizalde, A. G. Martínez, C. Morant and F. Márquez, *Am. Chem. Sci. J*., **3**, 178 (2013).
38. A. H. Mcheik and M. El Jamal, *J. Chem. Technol. Metallur*., **48**, 57 (2013).
39. Box GEP, Draper NR. Empirical Model-Building and Response Surfaces, Wiley, New York (1987).
40. B. Y. Chen, C. C. Hsueh, W. M. Chen and W. D. Li, *JTICE*, **42**, 816 (2011).
41. K. Ravikumar, S. Ramalingam, S. Krishnan and K. Balu, *Dyes Pigm.*, **70**, 18 (2006).
42. K. Ravikumar, S. Ramalingam, S. Krishnan and K. Balu, *Dyes Pigm.*, **72**, 66 (2007).
43. M. Cai, S. Wang and H. Liang, *Sep. Purif. Technol*., **100**, 74 (2012).
44. K. Sinha, P. D. Saha and S. Datta, *Dyes Pigm*., **94**, 212 (2012).
45. W. J. Chen, W. T. Su and H. Y. Hsu, *JTICE*, **43**, 246 (2012).
46. H. Jiao, W. Peng, J. Zhao and Ch. Xu, *Desalination*, **313**, 36 (2013).
47. K. Turhan, I. Durukan, S. A. Ozturkcan and Z. Turgut, *Dyes Pigm*., **92**, 897 (2012).
48. Montgomery DC. Design and Analysis of Experiments. Wiley, New York (2001).
49. Ch. Tizaouia and N. Grima, *Chem. Eng. J*., **173**, 463 (2011).
50. M. Rahimi, S. R. Shabanian and A. A. Alsairafi, *Chem. Eng. Process*., **48**, 762 (2009).
51. J. Ren, S. He, Ch. Ye, G. Chen and Ch. Sun, *Chem. Eng. J*., **210**, 374 (2012).
52. J. F. Chen, G. Z. Chen, J. X. Wang, L. Shao and P. F. Li, *AIChE J*., **57**, 239 (2011).
53. Y. Ku and L. K. Wang, *Ozone. Sci. Eng*., **24**, 133 (2002).
54. S. Aljbour, T. Tagawa and H. Yamada, *J. Ind. Eng. Chem*., **15**, 829 (2009).